Lineshapes in core-level photoemission from metals: II. $2H-TaS_2$ and its transition metal intercalates

1996 J. Phys.: Condens. Matter 8 1439

(http://iopscience.iop.org/0953-8984/8/10/015)

J. Phys.: Condens. Matter **8** (1996) 1439–1455. Printed in the UK

Lineshapes in core-level photoemission from metals: II. 2H-TaS_2 and its transition metal intercalates

H P Hughes and J A Scarfe

Cavendish Laboratory, University of Cambridge, Cambridge CB3 0HE, UK

Received 5 October, in final form 18 December 1995

Abstract. SHAPER, a computer package for x-ray photoemission lineshape analysis, is applied to experimental data on 2H-TaS_2 and some of its transition metal intercalates, revealing that charge transfer into the conduction band resulting from intercalation affects the core-level lineshape by modifying the density of states at the Fermi energy. The observations are discussed in terms of the rigid-band model of intercalation. In order to emphasize the interactive character of the fitting process, and its strengths and limitations, a range of fits of increasing complexity is presented.

1. Introduction

In paper [1], the computer package SHAPER was described and tested against artificial 'data' to demonstrate its capabilities for extracting reliable information about the electronic structure of the conduction bands of metallic systems from x-ray photoemission (XPS) core-level lineshapes. Here SHAPER is applied to experimental data obtained from 2H-TaS_2, a polytype of the layered metallic compound TaS_2; the sharp and intense Ta 4f photoemission lines, observed using synchrotron radiation, are particularly suitable for XPS lineshape studies. The materials can be intercalated, allowing the occupation of the conduction band to be increased and the effects on the lineshape, related to the band structure itself and to the transfer of charge from the intercalant atoms to the host material, observed systematically and directly.

2. 2H-TaS_2

TaS_2 adopts a layered structure, each layer consisting of a sheet of Ta atoms arranged hexagonally, sandwiched between two similar hexagonal sheets of S atoms such that each Ta atom is surrounded by six nearest-neighbour S atoms [2, 3], in either trigonal prismatic or octahedral co-ordination; the layers, of one or both types, stack in sequences to produce various polytypes. For 2H-TaS_2 the layers are all trigonal prismatic with a two-layer repeat along the direction normal to the layers. The principal electronic bonding is intralayer; interlayer bonding is weak, so the electronic structure is quasi-two-dimensional. The valence bands derive primarily from the S 3p states, with conduction bands of mainly Ta 5d character above; the lowest part of the d band is usually called the d_{z^2} band, with a gap to the $d_{xy;x^2-y^2}$ and $d_{xz;yz}$ bands above. For un-intercalated material the Fermi energy E_F lies approximately at the mid-point of the d_{z^2} band [2].

0953-8984/96/101439+17$19.50

The weak interlayer bonding allows other species of atoms or molecules to be intercalated between the layers, substantially modifying the properties of the host crystal. In particular, charge transfer between the host and the intercalant modifies the occupation of the d_{z^2} band, radically changing the host's electronic and optical properties [4]. The transition metal intercalates (TMIs) involving magnetic 3d ions—M_xTaS_2 ($x = \frac{1}{3}$ or $\frac{1}{4}$) exhibit regular superlattices for the 3d ions, with in-plane superlattice parameters parallel to the layers of $\sqrt{3}a$ and $2a$ respectively, where a is the host lattice parameter [5].

XPS measurements on the shallow Ta 4f core levels in 2H-TaS_2 are examined here in the light of model lineshape calculations based on the conduction band structure, as discussed in paper I. As was shown there, the excitation spectrum, $J(E)$, of the conduction band, is crucial, so knowledge of the conduction band density of states (DOS) for 2H-TaS_2 and its TMIs is required. Mattheiss's non-relativistic calculations [6] do not extend below the bottom of the Ta 5d band, while Guo and Liang's linear-muffin-tin-orbital method [7] and Blaha's linear-augmented-plane-wave method [8] should be more accurate and cover a wider energy range. These two calculations are largely in agreement, and show a sharply peaked d_{z^2} band separated from the remainder of the d band by about 1.3 eV. E_F lies approximately at the mid-point of the d_{z^2} band for pure 2H-TaS_2 which is therefore metallic; the two-dimensional Fermi surface gives rise to charge density wave (CDW) phenomena at low temperatures [9]. Overall, the conduction band structure could hardly be further removed from the flat DOS which is the basis of the Doniach-Sunjic (DS) lineshape [1].

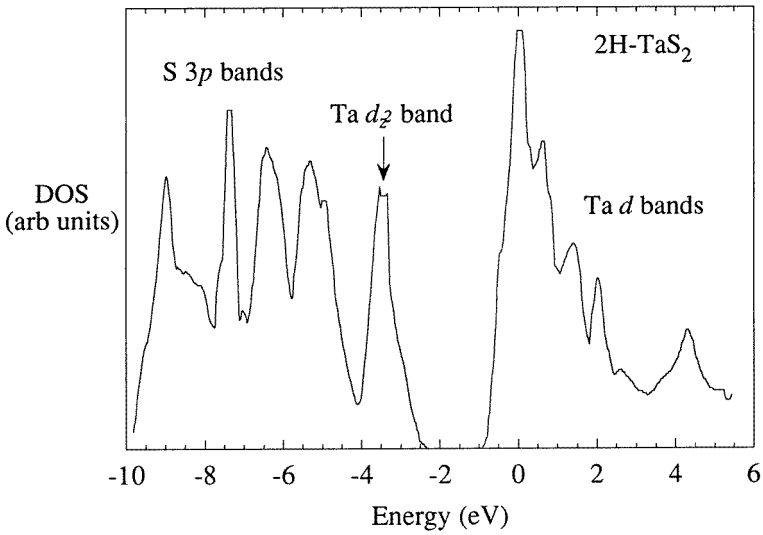

Figure 1. DOS states for the conduction band of 2H-TaS_2 (from Guo and Liang [7]).

Figure 1 shows the DOS for pure 2H-TaS_2, after Guo and Liang [7]; assuming that the d_{z^2} band is half full (occupied by one electron per formula unit), E_F lies at -3.35 eV, close to the d_{z^2} band peak. The rigid-band model (RBM) of intercalation suggests that the host band structure is largely unaltered upon intercalation, with E_F increasing to reflect the transfer of charge from the intercalant. The validity of this picture is supported by calculations for various intercalates of 2H-TaS_2; both Guo and Liang [7] and Blaha [8] calculate the DOS for 2H-$LiTaS_2$ and 2H-$SnTaS_2$, and for $LiTaS_2$ the RBM works well; recently Motizuki *et al* have also made spin-dependent calculations for $Mn_{\frac{1}{4}}TaS_2$ which

confirm this overall picture [10]. The RBM is further supported by XPS measurements of core-level binding energies [11], and by photoemission studies of the in-plane dispersion of the valence bands of similar materials [12, 13]; detailed synchrotron radiation photoemission measurements on Cs intercalation of VSe_2, which pick out the band dispersion in the z-direction perpendicular to the crystal layers, suggest that the dimensionality of the band structure changes from 3D to 2D as the layers are increasingly separated upon intercalation, but that the band structure in plane is not much affected [14].

The d_{z^2} band can hold two electrons per formula unit, so E_F can be found if the charge transfer is known. For the Mn and Co intercalates discussed here, the intercalants are known from paramagnetic susceptibility measurements [5] to be in a 2+ ionic state, suggesting that E_F moves to -3.21 eV for $M_{\frac{1}{4}}TaS_2$ and to -3.08 eV for $M_{\frac{1}{3}}TaS_2$. (Here M = Mn or Co.) The d_{z^2} DOS is sharply peaked, so band filling results in a marked reduction in $D(E_F)$, as Hall coefficient data [5] and calculations confirm [10]. This controllable DOS function makes 2H-TaS_2 and its TMIs an interesting set of materials to illustrate the effects the conduction band joint density of states (JDOS) has on XPS lineshapes.

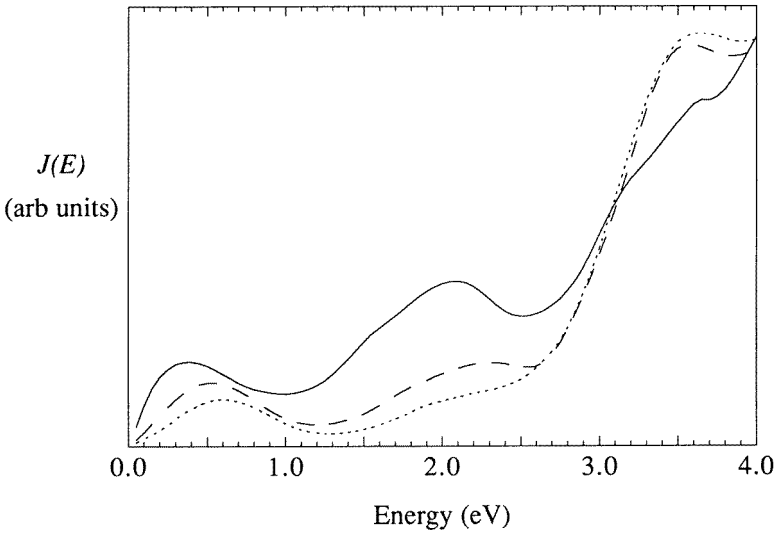

Figure 2. The JDOSs, $J(E)$, for the conduction bands of 2H-TaS_2 and its intercalates derived from the DOS of figure 1: ——, unintercalated 2H-TaS_2 ($E_F = -3.45$ eV); – – –, the same calculation with $E_F = -3.21$ eV to account for the charge transfer postulated in $M_{\frac{1}{4}}TaS_2$; ·····, $E_F = -3.08$ eV for $M_{\frac{1}{3}}TaS_2$. (M = Mn or Co.) No matrix element is included in the calculation.

Figure 2 shows the JDOS (in arbitrary units) calculated (equation (7), paper I) for the Guo and Liang DOS functions with E_F appropriate to 2H-TaS_2, $M_{\frac{1}{4}}TaS_2$ (charge transfer of $\frac{1}{2}$ electron per Ta), and $M_{\frac{1}{3}}TaS_2$ (charge transfer of $\frac{2}{3}$ electron per Ta), assuming the validity of the RBM and ignoring the symmetries of the bands and any matrix elements Λ. The JDOS functions are complex—$J(E)$ does not even approximate to the linear $J(E)$ that would produce a DS lineshape; but a lower asymmetry in the core-level lines is to be expected for $M_{\frac{1}{4}}TaS_2$ than for the host (and lower still for $M_{\frac{1}{3}}TaS_2$) because of the lower JDOS at $E = 0$.

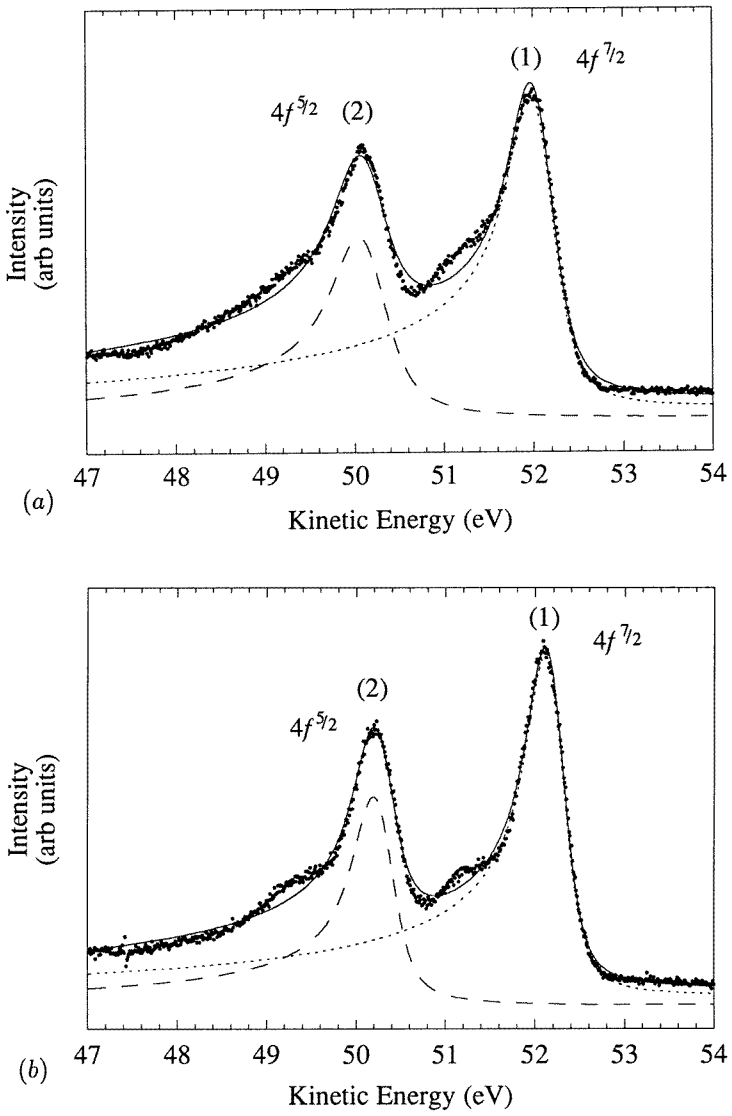

Figure 3. Representative electron kinetic energy distributions in the region of the Ta 4f emission for (*a*) 2H-TaS_2, (*b*) $Mn_{\frac{1}{4}}TaS_2$, (*c*) $Co_{\frac{1}{4}}TaS_2$ and (*d*) $Co_{\frac{1}{3}}TaS_2$. The data are shown as points and have been fitted with two DS lineshapes (JDOS-A). ——, total fit; · · · · · ·, $4f_{7/2}$ and – – –, $4f_{5/2}$ components. In this and later figures, each fitted component is shown superposed on the fitted background for display purposes, so the sum of the components does not match the total fit.

3. Experimental data

XPS measurements were made using synchrotron radiation (EPSRC Daresbury Laboratory, UK) with photon energies between 60 and 140 eV, concentrating on the Ta 4f levels, which have a high cross-section and a narrow linewidth; little variation in lineshape or binding energy with photon energy was observed, and the data used for analysis were

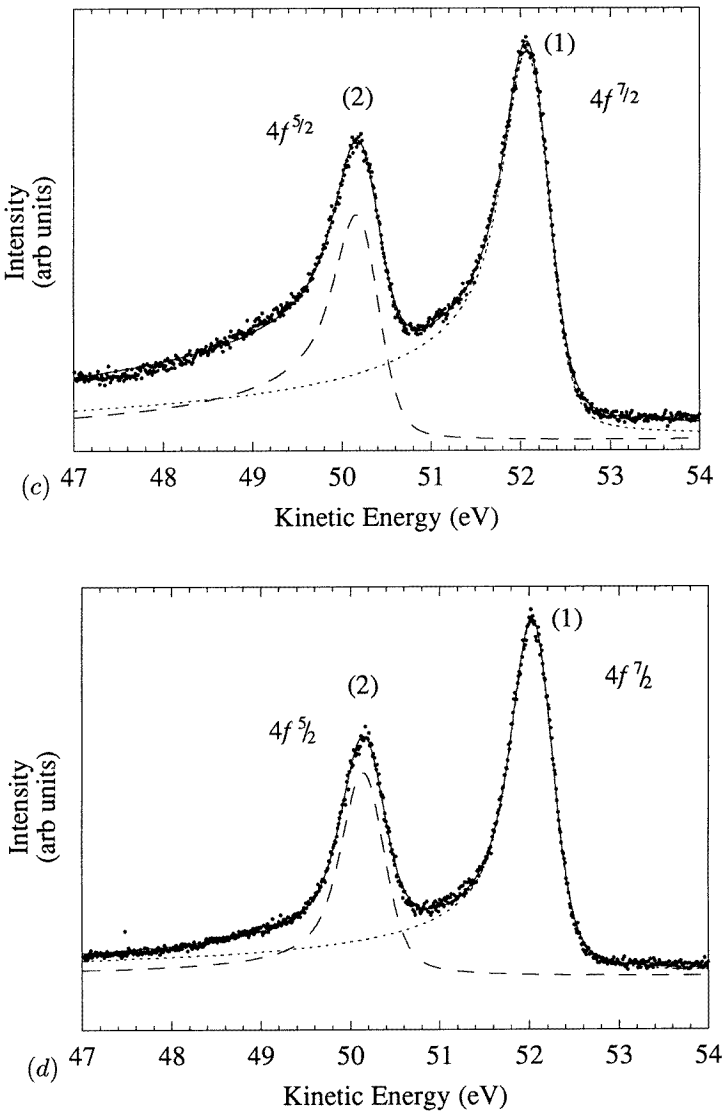

Figure 3. (Continued)

obtained with 70 and 80 eV photons, giving a good balance of resolution and signal-to-noise ratio. The photoelectrons were detected and analysed using a double-pass cylindrical mirror analyser (CMA). A representative spectrum for 2H-TaS_2 is shown in figure 3(*a*). The Ta 4f level produces a doublet, the spin–orbit split peaks corresponding to final states of angular momentum of $\frac{7}{2}$ and $\frac{5}{2}$ with multiplicities 8:6 (respectively peaks 1 and 2 in subsequent discussions), and each peak is clearly asymmetric with a pronounced tail to lower kinetic energy, and obvious shoulders; the tails extend for several electron volts, and that of the higher-KE peak extends under the lower-KE peak. Together with the underlying sloping background, these features make interpretation of the data without a detailed model of the lineshape almost impossible.

Similar representative 4f spectra for the TMIs, $Mn_{\frac{1}{4}}TaS_2$, $Co_{\frac{1}{4}}TaS_2$ and $Co_{\frac{1}{3}}TaS_2$, are also shown in figures 3(*b*)–(*d*) respectively. $Mn_{\frac{1}{4}}TaS_2$ differs from 2H-TaS_2 in that the 4f lines are less obviously asymmetric, and the shoulder at about 1 eV below each peak is more pronounced, while, despite its similar structure, $Co_{\frac{1}{4}}TaS_2$ has a radically different spectrum and the shoulders have all but disappeared. $Co_{\frac{1}{3}}TaS_2$ has a similar spectrum to that of $Co_{\frac{1}{4}}TaS_2$; there is possibly a shoulder in the tails ~ 0.2 eV below each peak, but the noise level makes it difficult to assess whether this feature is real.

4. Data analysis

The JDOS and $J(E)$ are used almost interchangeably in the following, implicitly assuming for now that the energy losses arise only from electron–hole pair excitations. The purpose of SHAPER is to determine the $J(E)$, the mathematical model used for fitting, consistent with the data, and values for the fitting parameters as set out in detail in paper I. The various model $J(E)$s used (JDOS-A, B, C and D) are shown schematically in figure 4, and will be described as they arise in the analysis.

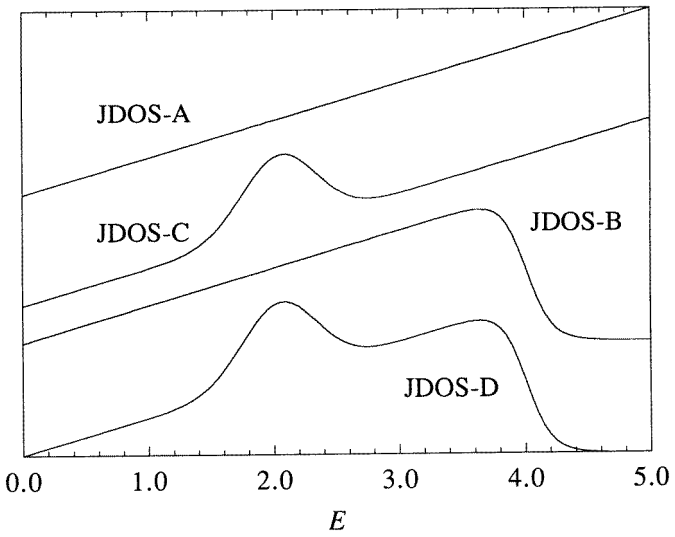

Figure 4. The forms used for $J(E)$ in fitting the data in this section. JDOS-A, B and C are all special cases of D, which is the full form of optd = 8 in SHAPER. The JDOSs, which are all zero at $E = 0$, have been displaced vertically for clarity.

It is usual in fitting XPS lineshapes for spin–orbit split doublets to assume that the asymmetry parameter α is the same for the two component lines. However, because of the different kinetic energies of the photoelectrons for each component, the details of the screening of the corresponding photoholes by the surrounding electrons will in principle be different, and this effect is likely to be more significant the greater spin–orbit splitting is as fraction of the overall kinetic energy; moreover, the angular momentum of the photoholes is different for the two components and, since the screening conduction electrons have mixed d and p character, this too may result in different screening for the two components. In all the fits which follow, therefore, it has been assumed that the α parameter for the spin–orbit split components of the Ta 4f levels may in principle be different.

Table 1. Fitting parameters obtained from SHAPER for the spectra shown in figures 3(*a*)–(*d*) using a two-peak fit and JDOS-A. In each case the instrumental width σ has been constrained to be the same for the $4f_{7/2}$ and $4f_{5/2}$ peaks. The energies of the peaks and their widths have units of electron volts.

	Peak	Amplitude	Energy	Lorentzian width (λ^{-1})	Gaussian width (σ)	α	ρ
2H-TaS_2	$4f_{7/2}(1)$	9000	52.06	0.265	0.345	0.364	6978
	$4f_{5/2}(2)$	4685	50.14	0.437		0.283	
$Mn_{1/4}TaS_2$	$4f_{7/2}(1)$	4757	52.18	0.216	0.307	0.337	4194
	$4f_{5/2}(2)$	2363	50.26	0.273		0.271	
$Co_{1/4}TaS_2$	$4f_{7/2}(1)$	1185	52.15	0.157	0.432	0.315	1288
	$4f_{5/2}(2)$	709	50.25	0.139		0.325	
$Co_{1/3}TaS_2$	$4f_{7/2}(1)$	665	52.08	0.150	0.413	0.210	1057
	$4f_{5/2}(2)$	285	50.17	0.214		0.117	

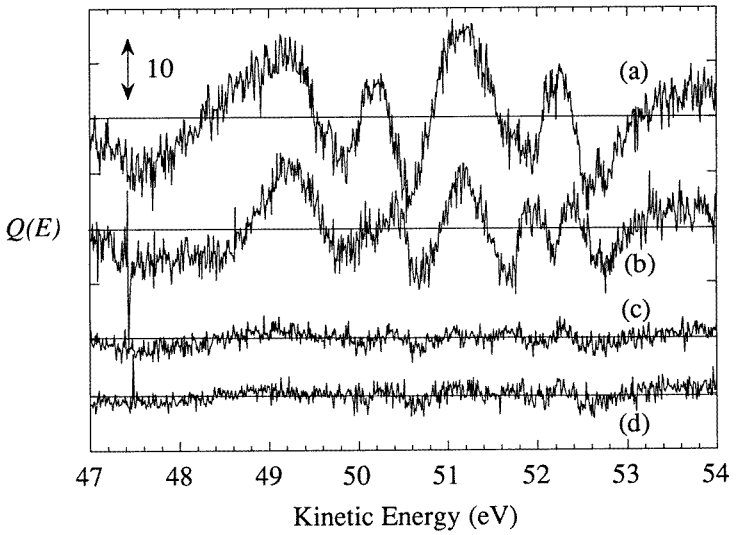

Figure 5. The normalized residual deviations $Q(E)$ for the spectra and fits in figure 3. Deviations above the general noise level are significant.

4.1. A first attempt at fitting the 4f lineshapes

It is obvious from the spectra that the DS lineshape cannot provide a good fit, but it is useful to attempt such a fit to see how the data deviate from it. Using $J(E) = \alpha E$ with the cut-off energy E_c set to a large value (JDOS-A in figure 4, appropriate for a DS lineshape) produces fits for 2H-TaS_2 and the intercalates as shown in figure 3(*a*)–(*d*); each shows the data $S(E)$, the best-fit model lineshape, $I(E)$, and the individual component lines. Table 1 gives the final values of the relevant parameters for each peak, including the goodness-of-fit parameter ρ, but the parameters characterizing the background are not shown for brevity.

Figure 5 summarizes the normalized residuals $Q(E)$, given by

$$Q(E) = [S(E) - I(E)]/\sqrt{S(E)}. \tag{1}$$

Since the different datasets have different signal-to-noise ratios, this forms a useful graphical comparator for the qualities of the fits. Figures 3(a) and 5(a) show that the DS lineshape is clearly inadequate for 2H-TaS_2 in that (i) the shoulders at $\sim$ 1 eV below the peaks are not accounted for, (ii) the tail of the model extends too far to low E, the data falling below the model between 50.5 and 51.0 eV and between 47.0 and 48.5 eV and (iii) the fit around the top of the peaks is poor, probably because the model peaks are shifted slightly to compensate for inadequacies of the fit elsewhere. Figures 3(b) and 5(b) show that the outcome is broadly similar for $Mn_{\frac{1}{4}}TaS_2$. However the fits of the $Co_{\frac{1}{4}}TaS_2$ data (figures 3(c) and 5(c)) are more successful, though the fit is not perfect around the top of the peak, and the tail again seems to be too high in the region 47.5–48.5 eV with the background reduced to compensate. For $Co_{\frac{1}{3}}TaS_2$ (figures 3(d) and 5(d)) the fit appears even better; the only discrepancy appears in the tail of the lower-KE peak, where again the tail extends too far to low KE. A consistent trend is that the asymmetry of the higher-KE peak (1) is greater than that of the lower-KE peak (2), but it will be demonstrated below that that this is the consequence of the inappropriate $J(E)$ used here. The ideal value of ρ in each case should be 690, so the fits are clearly inadequate in general terms; the general inconsistency of the α values and of the Lorentzian widths in table 1 should also be noted, again reflecting the inadequacy of the overall fit.

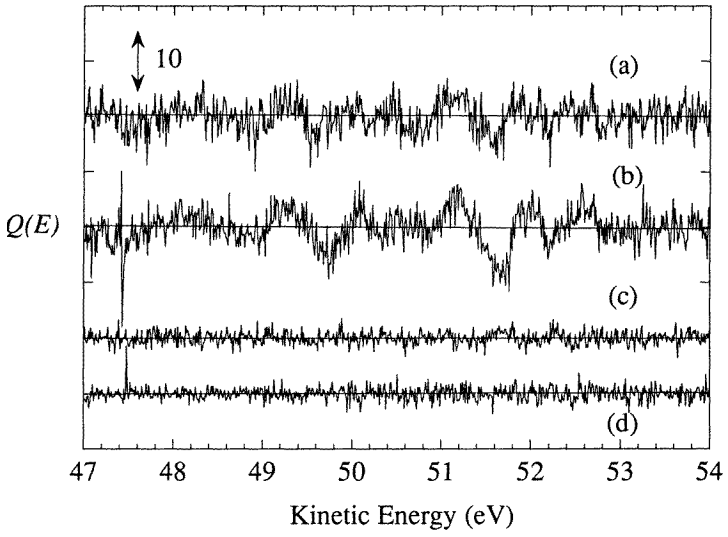

Figure 6. The normalized residual deviations $Q(E)$ for the spectra in figure 3 fitted to JDOS-B as discussed in the text.

A simple DS lineshape is therefore inadequate for a full interpretation of these data, and it is tempting at this point to construct a JDOS for $J(E)$ like those in figure 2 for each material from the DOSs in figure 1; but, as emphasized in paper I, the lineshape depends explicitly on the excitation spectrum, $J(E)$, and only indirectly on the DOS, $D(E)$, so a number of different $D(E)$ forms could produce the same lineshape. It is therefore appropriate at this stage to attempt to find a suitable $J(E)$, albeit empirically, before going on to discuss

Table 2. Fitting parameters obtained from SHAPER for the spectra shown in figure 3(*a*)–(*d*) using a two-peak fit and JDOS-D. In each case the instrumental width σ and the parameters for the added peak in JDOS-D (position, width and ratio of its amplitude to the JDOS slope at $E = 0$), and the cut-off position, have been constrained to be the same for the $4f_{7/2}$ and $4f_{5/2}$ peaks. The JDOS cut-off sharpness is fixed at 5.0 in all fits. Parameter values marked * have reached an upper or lower bound introduced to prevent wild excursions in the fitting process.

	Peak	Amplitude	Energy	Lorentzian width (λ^{-1})	Gaussian width (σ)	α	Cut-off position	Cut-off sharpness	JDOS peak position	JDOS peak width	JDOS peak/slope ratio	ρ
2H-TaS_2	$4f_{7/2}(1)$ $4f_{5/2}(2)$	3828 2392	52.07 50.18	0.036 0.001*	0.495	0.139 0.146	3.86	5.0	0.77	0.43	3.14	854
$Mn_{1/4}TaS_2$	$4f_{7/2}(1)$ $4f_{5/2}(2)$	1866 1276	52.13 50.24	0.025 0.017	0.495	0.107 0.118	3.32	5.0	0.88	0.31	3.65	779
$Co_{1/4}TaS_2$	$4f_{7/2}(1)$ $4f_{5/2}(2)$	627 330	52.16 50.26	0.059 0.018	0.475	0.308 0.299	3.52	5.0	0.40	0.04	0.86	788
$Co_{1/3}TaS_2$	$4f_{7/2}(1)$ $4f_{5/2}(2)$	372 211	52.09 50.19	0.032 0.044	0.484	0.137 0.119	1.82	5.0	0.69	1.30	0.68	739

the corresponding DOS. In attempting to improve the fits to the data, various tests with other $J(E)$s of figure 4 were made, but the complete outcome of each fit is not shown graphically for reasons of space; instead the quality of fit is assessed through plots of the residual deviations $Q(E)$ between the data and each fit, together with the tabulated output parameters.

The simplest modification of $J(E)$ is to introduce a cut-off at an energy of a few electron volts—JDOS-B—creating a corresponding but smoother cut-off in the core-level line itself, as observed; the fits are much improved. Figure 6(a) shows the result for 2H-TaS_2; there are still some systematic deviations in the residuals, but the fit around the tops of the peaks is much better though the shoulder is not fully accounted for. $J(E)$ shows that the optimal JDOS has a smooth rather than a sharp cut-off, and reaches a maximum at about 1.3 eV, slightly more than the peak/shoulder separation; $J(E)$ for each peak has the same shape, but α is again permitted to be different. The fit for $Mn_{\frac{1}{4}}TaS_2$ (figure 6(b)) shows a less marked improvement—even with the sharply cut off JDOS the model cannot reproduce a feature as sharp as the shoulder observed in the data—but for $Co_{\frac{1}{4}}TaS_2$ (figure 6(c)) the fit is very much improved, and that for $Co_{\frac{1}{3}}TaS_2$ (figure 6(d)) is excellent.

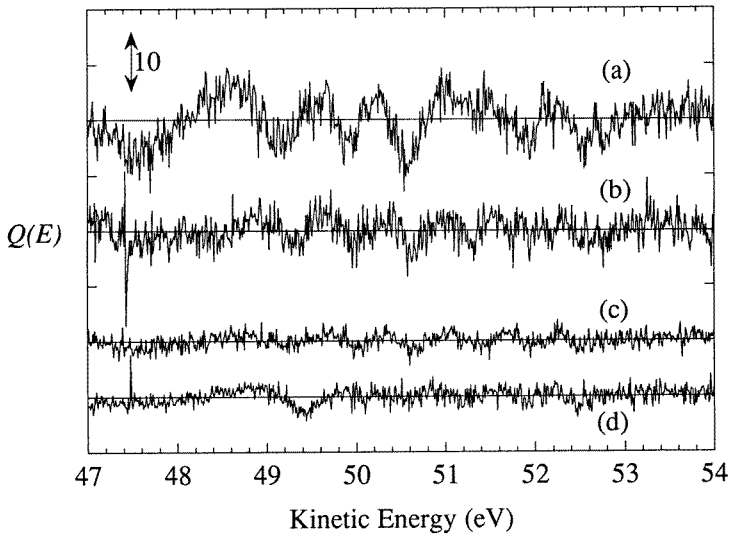

Figure 7. The normalized residual deviations $Q(E)$ for the spectra in figure 3 fitted to JDOS-A, using four fitting peaks, as discussed in the text.

An obvious way to improve the fits is to treat the problem as a four-peak fit, an approach often used to include known or suspected satellite peaks in the lineshape. This introduces extra free parameters, but surprisingly the results (figure 7) are unimpressive. JDOS-A was used again, with the constraints that the α values of each main peak (1 and 2) and its satellite (3 and 4), and their Lorentzian widths, are equal. ρ-values for these fits, except for $Mn_{\frac{1}{4}}TaS_2$, are higher than those for JDOS-B (table 1), and are all much lower than those obtained from the more successful fits detailed in subsection 4.2 below, despite the extra free parameters, so simply including more parameters does not elucidate the physics of the system; only a carefully refined model for $J(E)$ will improve the fit. The JDOSs of 2H-TaS_2 and its TMIs are too complicated for the core-level lines to be fitted by a simplistic lineshape that does not take the form of $J(E)$ into account.

4.2. A better fit to the 4f lineshapes

It seems that a $J(E)$ that increases no faster than linearly with E cannot reproduce the shoulders seen for 2H-TaS_2 and particularly of $Mn_{\frac{1}{4}}TaS_2$; an explicit peak in $J(E)$ must be introduced using the more complicated $J(E)$ functions available in SHAPER.

Initially, a $J(E)$ of the form αE plus a Gaussian peak is taken—JDOS-C (see figure 4). To reduce the number of variables, the 'cut-off' is set very high (effectively infinity), as in the first set of fits with JDOS-A. The residuals of the fits, obtained using optd= 8 in SHAPER, are shown in figure 8; for 2H-TaS_2 there is clearly an improvement, and ρ is reduced to 906. (The 'target' value is 702 (data points)−19 (free parameters), i.e. 683, though error assessment is difficult and only a slight underestimate ($\sim$ 10%) would bring the fit into a statistically acceptable range.) The greatest improvement is for $Mn_{\frac{1}{4}}TaS_2$—the shoulders are fitted almost perfectly. It is still not possible to say that there are no trends in the residuals, but further attempts to improve the fit will require extra, seemingly arbitrary, parameters. (The $Co_{\frac{1}{3}}TaS_2$ and $Co_{\frac{1}{4}}TaS_2$ fits, however, show no improvement over those for a JDOS that simply cuts off (figure 7(*c*) and (*d*)); empirically, this is because the peaks for the Co intercalates do not exhibit low-KE shoulders—see below.)

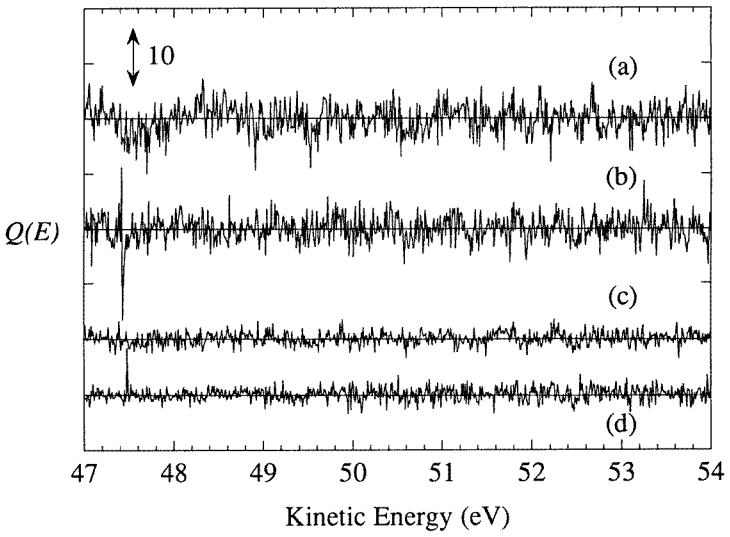

Figure 8. The normalized residual deviations $Q(E)$ for the spectra in figure 3 fitted to JDOS-C as discussed in the text.

For completeness, the model $J(E)$ with a peak is combined with a cut-off—JDOS-D (figure 4), and the fits are expected to be at least as good as any obtained so far, though the number of free parameters has been increased still further. These final fits to the data are shown in figure 9, the residuals in figure 10 and the output parameters in table 2; the corresponding model JDOSs are set out in figure 11 and show remarkable consistency between the parameters obtained for the two component peaks in the 4f doublet. Table 3 summarizes values of ρ for all the fits. Increasing the number of free parameters can be counterproductive in introducing unphysical complexity—the fits using JDOS-D rather than JDOS-C are only marginally better for most datasets—and the purpose of ρ is to locate objectively the point at which this occurs, but a problem lies in assessing the error values, η_i, representing the standard deviation of the noise for each data point, since small, consistent

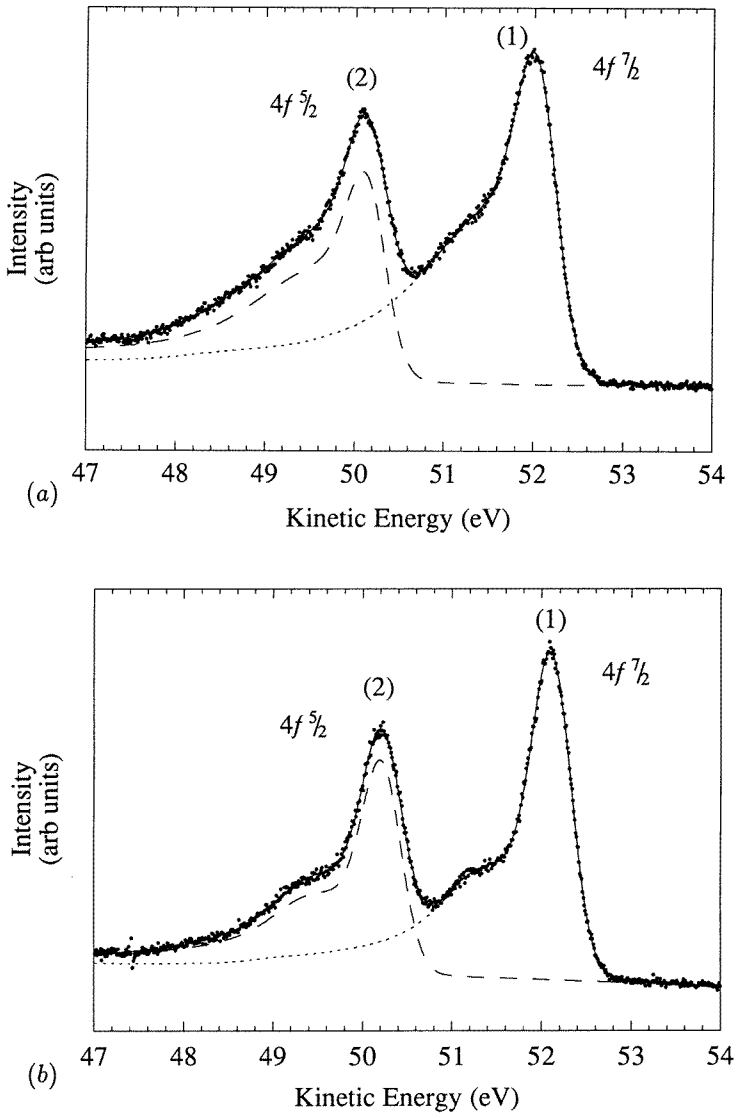

Figure 9. The electron kinetic energy distributions as in figure 3 for (*a*) 2H-TaS_2, (*b*) $Mn_{\frac{1}{4}}TaS_2$, (*c*) $Co_{\frac{1}{4}}TaS_2$ and (*d*) $Co_{\frac{1}{3}}TaS_2$. The data have been fitted with two lineshapes corresponding to JDOS-D as discussed in the text. ——, total fit; · · · · · ·, $4f_{7/2}$ and – – –, $4f_{5/2}$ components.

under- or over-estimates can put ρ outside acceptable limits, so relative improvements in ρ, rather than absolute values, are important. It seems from table 3 that a sufficiently good fit is reached with JDOS-B for the Co intercalates and with JDOS-C for the others. $Co_{\frac{1}{3}}TaS_2$ is particularly interesting in this respect; ρ is *higher* for a fit with JDOS-D than for JDOS-B, even though JDOS-D has more free parameters and JDOS-B is a subset of JDOS-D (with the height of the Gaussian peak set to zero). The problem involves local minima in the extra dimensional parameter space afforded by JDOS-D.

The best-fit $J(E)$s for each material can be identified from table 3 as JDOS-D for 2H-

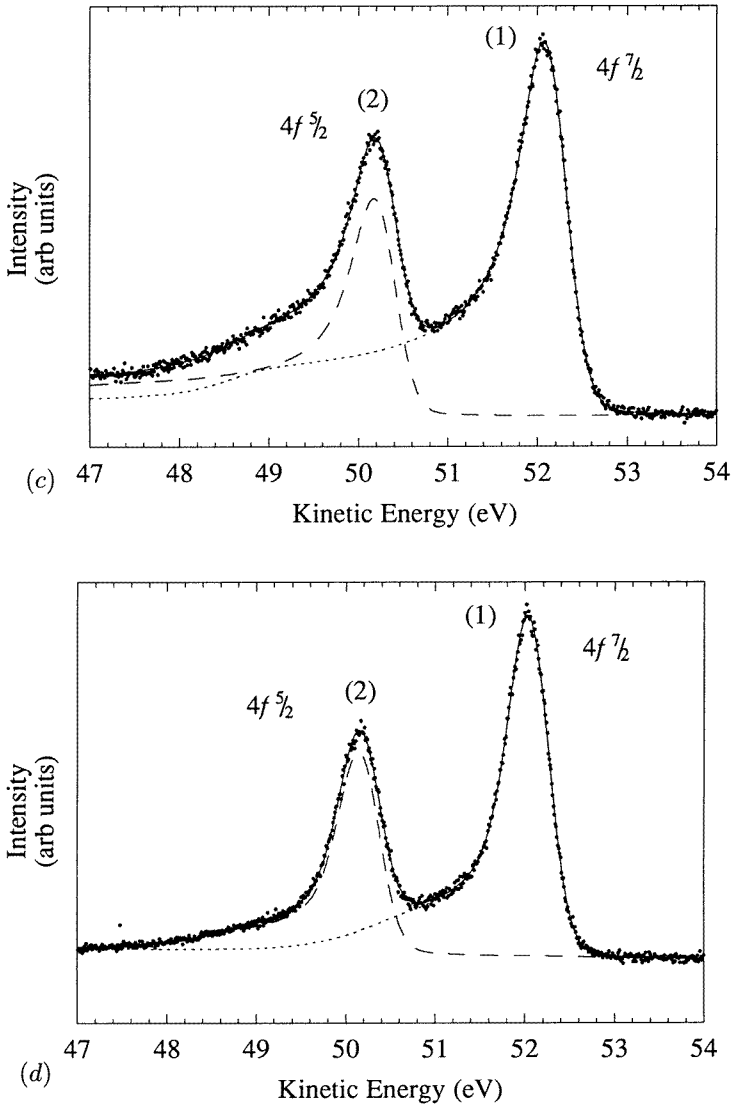

Figure 9. (Continued)

TaS_2 and $Mn_{\frac{1}{4}}TaS_2$ (figures 11(*a*) and (*b*)), but because the peak introduced in JDOS-D was inappropriate for the Co intercalates and did not improve the goodness of fit, JDOS-B is more appropriate for $Co_{\frac{1}{4}}TaS_2$ and $Co_{\frac{1}{3}}TaS_2$. $J(E)$ for 2H-TaS_2 has the highest slope at the origin, and a broad peak near 1.0–1.5 eV. $J(E)$ for $Mn_{\frac{1}{4}}TaS_2$ has a lower initial slope, but rises steeply from ~ 0.5 eV to a much sharper peak at almost exactly 1 eV. The behaviour of any of these $J(E)$ results beyond the Gaussian peak (i.e. beyond 1.5–2.0 eV) is unreliable as $J(E)$ in this range has little effect on the lineshape. $J(E)$ for $Co_{\frac{1}{4}}TaS_2$ is markedly different; while the initial slope is similar to that for 2H-TaS_2, the JDOS falls away at about 1.5 eV rather than rising to a peak. $J(E)$ for $Co_{\frac{1}{3}}TaS_2$ is anomalous in that the lower-KE peak has a lower asymmetry (slope of $J(E)$ at low E) than its higher-KE

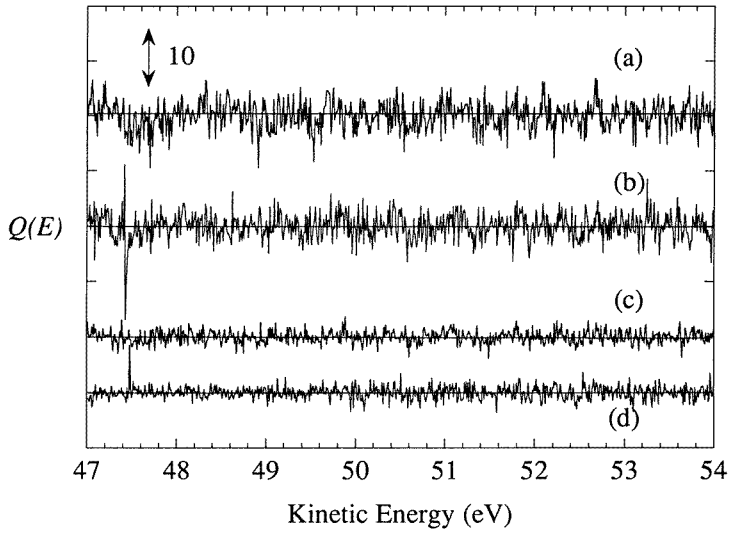

Figure 10. The normalized residual deviations $Q(E)$ for the spectra in figure 3 fitted to JDOS-D as discussed in the text.

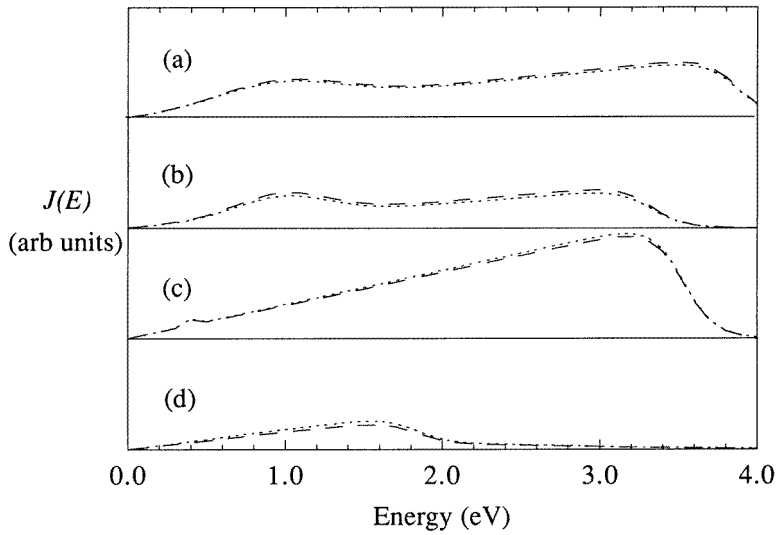

Figure 11. The model JDOSs for (*a*) 2H-TaS_2, (*b*) $Mn_{\frac{1}{4}}TaS_2$, (*c*) $Co_{\frac{1}{4}}TaS_2$ and (*d*) $Co_{\frac{1}{3}}TaS_2$, corresponding to the output parameters in table 2 for peak 1 (· · · · · ·) and peak 2 (– – –).

partner; it seems unlikely that this has physical significance, as discussed in subsection 4.1. The value of $J(E)$ is low at low E as for $Mn_{\frac{1}{4}}TaS_2$, but stays low, and does not fall off as quickly at higher E.

The insensitivity of the lineshape to $J(E)$ at higher energies limits this potentially powerful technique for deriving the conduction band structure, but without such a method analysis would be limited to, at best, an inappropriate DS lineshape providing an 'average'

Table 3. Summary of the goodness-of-fit parameters ρ obtained by fitting with the various JDOS models outlined in the text. The ideal ρ value is given by the number of data points (702 for each spectrum) minus the number of free parameters in the fit. Other datasets analysed but not shown here produced very similar results. The best fit for each material is marked *; for the Co intercalates, the fits marked † are as good, but the JDOS used is less physically appropriate.

	JDOS-A DS line	JDOS-B Linear JDOS with smooth cut-off	JDOS-A (two lines) Double DS line	JDOS-C Linear JDOS with Gaussian peak	JDOS-D Linear JDOS with smooth cut-off + Gaussian peak
Figures	3, 5	6, 7	8	9, 10	11–13
Ideal ρ value	690	689	684	687	685
2H-TaS_2	6978	1000	2055	906	854*
$Mn_{\frac{1}{4}}TaS_2$	4194	1466	975	781	779*
$Co_{\frac{1}{4}}TaS_2$	1288	787*	1023	820	788†
$Co_{\frac{1}{3}}TaS_2$	1057	736*	1147	749	739†

fit. This would yield an asymmetry parameter α that, because all data-points are given equal weight, would not reflect the JDOS in the low-E region where most can be deduced from the core-level line. The quality of the fitted results depends on the experimental resolution and signal-to-noise ratio of the data.

5. Discussion—the JDOS in 2H-TaS_2

The two forms of $J(E)$ suggested by band structure calculations and from fitting the core-level lineshapes are quite different in shape, but have some common features. Both are complex, far from the linear $J(E)$ implicit in the DS lineshape, and as the concentration of intercalant is increased the initial slope of $J(E)$ decreases.

With E_F in the correct position for 2H-TaS_2, there is a peak at about 0.4 eV in the theoretical $J(E)$ (figure 2), another at $\sim$ 2 eV, and a definite trough at $\sim$ 1 eV. As the intercalant concentration increases, $J(E)$ decreases for all E and the peaks move to higher E and are less pronounced. This contrasts with the results of subsection 4.2, in which the strongest peak in $J(E)$ is at $\sim$ 1 eV for $Mn_{\frac{1}{4}}TaS_2$ with a similar but slightly weaker and broader peak for 2H-TaS_2. For the Co_xTaS_2 intercalates, the peak has all but disappeared, despite the RBM's prediction that the JDOSs for $Co_{\frac{1}{4}}TaS_2$ and $Mn_{\frac{1}{4}}TaS_2$ are the same. Clearly the situation is more complicated than so far envisaged.

The discrepancy between the fitted $J(E)$ for 2H-TaS_2 and the calculated JDOS implies that the deficiency is more than the inability of the RBM to explain the effect of intercalation. The RBM indeed explains the trend in the slope of $J(E)$ at low E throughout the intercalate series—with the triangular shaped d_{z^2} band half filled in 2H-TaS_2, charge transfer into the conduction band must reduce the density of states at E_F, and thus decrease the initial slope of the JDOS, as borne out by figure 2.

Reconciling the $J(E)$ retrieved from lineshape fitting with the physics of the 2H-TaS_2 intercalate family requires consideration of the basic processes of photoelectron energy loss. The formation of electron–hole pairs is the most obvious source of *low*-energy excitations when the core-level hole is formed, but plasmon excitations, both intrinsic and extrinsic,

can also occur, and, if the plasmon energy is low, could contribute to the spectrum of possible final states. Extrinsic plasmon loss is usually addressed using the dielectric energy loss function, but intrinsic losses must be treated as a contribution to $J(E)$. The matrix elements will be quite different from those for electron–hole pair formation, but the two mechanisms can still be combined into a single $J(E)$, with the plasmon represented by a peak to the JDOS which has so far reflects only electron–hole pair formation. $J(E)$ then becomes the density of all excitations, not just the JDOS. Intrinsic and extrinsic plasmon losses cannot easily be separated, but both can be treated semi-empirically by adding a narrow peak to $J(E)$; the most informative parameter is the energy of the peak, which can be related to the electron energy loss spectrum observed by complementary techniques.

The plasmon excitations available in 2H-TaS_2 and its TMIs can be obtained from reflectivity spectra, and, where available, the derived dielectric functions. For 2H-TaS_2 Beal *et al* [15] found a sharp peak ($\sim$ 0.3 eV wide) at $\sim$ 1 eV corresponding to that in $J(E)$ for the best fits. Parkin and Beal [16] measured the reflectivity of some TMIs relevant here, each exhibiting a dip near 1–1.5 eV, indicating an absorption; the sharpest dip is for $Mn_{\frac{1}{4}}TaS_2$, with a smoother trough centred at higher energy in unintercalated 2H-TaS_2; for $Co_{\frac{1}{3}}TaS_2$ the feature is very much broader, and shifted to even higher energy. Without a Kramers–Krönig analysis it is not possible to be specific about energies, but the trend in the excitation spectrum should carry over into the $J(E)$ obtained from the XPS data. Recall that in the successful fits of subsection 4.2 it was the Mn intercalate that had the strongest and sharpest peak in $J(E)$, with the peak in the 2H-TaS_2 being broader and at higher energy. In $Co_{\frac{1}{3}}TaS_2$, $J(E)$ has no significant peak at all, and continues to rise gently with no sharp feature.

The trend in the slope of $J(E)$ at low E for 2H-TaS_2 through $Mn_{\frac{1}{4}}TaS_2$ to $Co_{\frac{1}{3}}TaS_2$ is loosely consistent with the RBM, with charge transfer into the d_{z^2} band reducing $D(E_F)$, but the complexity of $J(E)$ obtained from SHAPER and of the calculated JDOS [7] makes it inappropriate to compare values of α from $J(E)$ directly with the experimental predictions. ($J(E)$ is dimensionaless and includes an unknown matrix element; though this could be assumed to be the same for all four materials, the discussion would be limited to a comparison of the *ratios* of the initial slopes in the JDOSs.) The trend in the positions and widths of the superimposed peak (absent for the Co intercalates) in $J(E)$ accords with the positions and widths of reflectivity minima [16]. In Parkin and Beal's analysis, the question of why the reflectivity minimum is shifted down in $Mn_{\frac{1}{4}}TaS_2$ and up in $Co_{\frac{1}{3}}TaS_2$ is left largely unanswered, though it clearly indicates a deficiency of the RBM in this case. A further deficiency is indeed obvious from the data for $Mn_{\frac{1}{4}}TaS_2$ and $Co_{\frac{1}{4}}TaS_2$ shown in figure 3(*b*) and (*c*); whereas the total charge transfer in both cases should be the same, the spectra are notably different away from the sharp peaks themselves. So while the RBM can in general terms account for the changes in asymmetry parameter (determined principally from the region of the spectra close to the peaks themselves) observed on intercalation, it does not provide a complete description of the effect of intercalation on the band structure of the host material.

6. Conclusion

The Ta 4f core-level XPS lineshapes for 2H-TaS_2 and its TMIs are consistent with the conduction band electronic structure and the effects of the charge transfer into the conduction band associated with intercalation. This validates the technique of core-level lineshape analysis set out here, at least close to the lineshape peak itself; the determination of band structure effects further away from the peak is relatively inferior because of the decreasing

sensitivity of the lineshape to higher-energy features in the effective joint density of states. The data also confirm the general applicability of the RBM for these two-dimensional materials, though in detail it does not provide a complete description.

Acknowledgments

This work was supported by the UK Engineering and Physical Science Research Council. The authors also gratefully acknowledge the assistance of the staff of the Synchrotron Radiation Facility at the EPSRC Daresbury Laboratory, particularly Dr F Quinn and Dr D Law.

References

[1] Hughes H P and Scarfe J A 1996 *J. Phys.: Condens. Matter* 1421–38
[2] Wilson J A and Yoffe A D 1969 *Adv. Phys.* **18** 193
[3] Beal A R 1979 *Intercalated Layered Materials* (Dordrecht: Reidel)
[4] Friend R H and Yoffe A D 1987 *Adv. Phys.* **36** 1
[5] Parkin S S P and Friend R H 1980 *Phil. Mag.* B **41** 65
[6] Mattheiss L F 1973 *Phys. Rev.* B **8** 3719
[7] Guo G Y and Liang W Y 1987 *J. Phys. C: Solid State Phys.* **20** 4315
[8] Blaha P 1991 *J. Phys.: Condens. Matter* **3** 9381
[9] Wilson J A, di Salvo F J and Mahajan S 1975 *Adv. Phys.* **24** 117
[10] Motizuki K, Suzuki N and Tomishima S 1992 *J. Magn. Magn. Mater.* **104** 681
[11] Barry J J and Hughes H P 1982 *J. Phys. C: Solid State Phys.* **15** L797
[12] Clark W B 1976 *J. Phys. C: Solid State Phys.* **9** L693
[13] Barry J J and Hughes H P 1983 *J. Phys. C: Solid State Phys.* **16** 5393
[14] Starnberg H I, Brauer H E, Holleboom L J and Hughes H P 1993 *Phys. Rev. Lett.* **70** 3111
[15] Beal A R, Hughes H P and Liang W Y 1975 *J. Phys. C: Solid State Phys.* **8** 4236
[16] Parkin S S P and Beal A R 1980 *Phil. Mag.* B **42** 627